Spectroscopic Studies of the Corrinoid/Iron −Sulfur Protein from Moorella thermoacetica

6 AUTHORS, INCLUDING:

Javier Seravalli
University of Nebraska at Lincoln
51 PUBLICATIONS **1,434** CITATIONS

Thomas Spiro
Princeton University
275 PUBLICATIONS **9,334** CITATIONS

Stephen W Ragsdale
University of Michigan
201 PUBLICATIONS **7,505** CITATIONS

Thomas C Brunold
University of Wisconsin–Madison
102 PUBLICATIONS **3,915** CITATIONS

Spectroscopic Studies of the Corrinoid/Iron–Sulfur Protein from *Moorella thermoacetica*

Troy A. Stich[†], **Javier Seravalli**[‡], **Swarnalatha Venkateshrao**[§], **Thomas G. Spiro**[§], **Stephen W. Ragsdale**[‡], and **Thomas C. Brunold**

[†]Department of Chemistry, University of Wisconsin-Madison, Madison, Wisconsin 53706

[‡]Department of Biochemistry, University of Nebraska, Lincoln, Nebraska 68588

[§]Department of Chemistry, Princeton University, Princeton, New Jersey 08544

Abstract

Methyl transfer reactions are important in a number of biochemical pathways. An important class of methyltransferases uses the cobalt cofactor cobalamin, which receives a methyl group from an appropriate methyl donor protein to form an intermediate organometallic methyl–Co bond that subsequently is cleaved by a methyl acceptor. Control of the axial ligation state of cobalamin influences both the mode (i.e., homolytic vs heterolytic) and the rate of Co–C bond cleavage. Here we have studied the axial ligation of a corrinoid iron–sulfur protein (CFeSP) that plays a key role in energy generation and cell carbon synthesis by anaerobic microbes, such as methanogenic archaea and acetogenic bacteria. This protein accepts a methyl group from methyltetrahydrofolate forming Me–Co^{3+}CFeSP that then donates a methyl cation (Me) from Me–Co^{3+}CFeSP to a nickel site on acetyl-CoA synthase. To unambiguously establish the binding scheme of the corrinoid cofactor in the CFeSP, we have combined resonance Raman, magnetic circular dichroism, and EPR spectroscopic methods with computational chemistry. Our results clearly demonstrate that the Me–Co^{3+} and Co^{2+} states of the CFeSP have an axial water ligand like the free $MeCbi^+$ and $Co^{2+}Cbi^+$ cofactors; however, the Co–OH_2 bond length is lengthened by about 0.2 Å for the protein-bound cofactor. Elongation of the Co–OH_2 bond of the CFeSP-bound cofactor is proposed to make the cobalt center more "Co^{1+}-like", a requirement to facilitate heterolytic Co–C bond cleavage.

Introduction

A number of anaerobic microbes, including archaea and bacteria, utilize the autotrophic Wood–Ljungdahl pathway to generate cell carbon and energy from CO_2 and CO.[1] This pathway consists of two separate branches: the methyl branch, in which five enzymes catalyze the reduction of CO_2 to the methyl group of 5-methyltetrahydrofolate (CH_3–H_4folate); and the carbonyl branch, wherein the methyl group of CH_3–H_4folate, CO_2, and Coenzyme A are converted to acetyl-CoA by the bifunctional $\alpha_2\beta_2$ tetrameric enzyme termed carbon monoxide dehydrogenase/acetyl-coenzyme A synthase (CODH/ACS). CODH/ACS is equipped with multiple metal cofactors that serve as electron-transfer centers and/or catalytic sites. Each β-subunit (CODH) houses a unique [Ni Fe]:[Fe_3S_4] reaction center,[2] termed the C-cluster, which serves as the site for CO_2 reduction. The resulting CO product is shuttled from CODH through an intramolecular tunnel to an equally unique [Ni_2–Fe_4S_4] center called the A-cluster, which is located in ACS, the α-subunit.[3-5] Here this CO molecule combines with a methyl group donated to the A-cluster by a corrinoid/FeS protein (CFeSP, Scheme 1) to yield a Ni-bound

acetyl group that is then attacked by the thiolate group of the cosubstrate CoA to generate the acetyl-CoA product.[6]

The 83 kDa heterodimeric CFeSP that delivers the methyl group to the ACS active site (i.e., the A-cluster) (Scheme 1) employs the corrinoid cofactor methyl-Co^{3+}-5-methoxybenzimidazolylcobamide (Factor III_m, Figure 1)[7,8] that is bound to the 35 kDa subunit of this enzyme.[9] The structure of Factor III_m is nearly identical to that of the methylcobalamin (MeCbl) cofactor employed by methionine synthase (MetH);[10] however, in contrast to the 5,6-dimethylbenzimidazole/nucleotide loop assembly found in MeCbl, Factor III_m employs a 5-methoxybenzimidazolyl (MBI) nitrogen base that is tethered to the corrin ring at C^{17} through a propionamide linkage.[11] When extracted from the CFeSP, the isolated cofactor is coordinated in the lower axial position by MBI. Interestingly, though, electron paramagnetic resonance (EPR) and electronic absorption (Abs) studies of CFeSP revealed that this base is no longer ligated to the central Co ion when the cofactor is bound to the protein.[12]

Methylation of the bound corrinoid to yield Me–Co^{3+}CFeSP is catalyzed by a methyltransferase (MeTr, Scheme 1), where the methyl group derives from CH_3–H_4folate originating from the methyl branch of the Wood–Ljungdahl pathway. During catalytic turnover, the Me–Co^{3+}CFeSP formally transfers a methyl cation to the ACS A-cluster through heterolytic cleavage of the Co–C bond, resulting in the formation of a transient Co^{1+} corrinoid species that is subsequently remethylated by MeTr. However, the $Co^{2+/1+}$ reduction potential of the CFeSP-bound corrinoid is very negative, $E° = –504$ mV,[13] leading to oxidation of the Co^{1+} intermediate to the catalytically inactive Co^{2+} state about 1 out of every 100 turnovers. [14] Intriguingly, metal analysis as well as Mössbauer and EPR spectroscopic studies revealed that the 48 kDa subunit of CFeSP contains a $[Fe_4S_4]$ cluster that functions to reduce the Co^{2+} form of the corrinoid back to the active Co^{1+} state.[12,14,15] The $[Fe_4S_4]^{2+/1+}$ reduction potential of this cluster is $E° = –523$ mV, which is nearly isopotential with the $Co^{2+/1+}$ couple of the corrinoid. Removal of Factor III_m from the CFeSP by treatment with urea has no noticeable effect on the Mössbauer and EPR properties of the $[Fe_4S_4]$ cluster and raises the $[Fe_4S_4]^{2+/1+}$ reduction potential by a mere ~6 mV. Likewise, the addition of mersalyl acid, which disrupts the $[Fe_4S_4]$ cluster without perturbing the EPR spectrum of the CFeSP-bound Co^{2+}corrinoid cofactor, has negligible effects on the midpoint potential of the $Co^{2+/1+}$ couple, demonstrating that the two metal cofactors are electronically uncoupled.[13]

While the functional roles of both metal cofactors in CFeSP are well understood, fundamental questions concerning the exact nature of the coordination environment of the corrinoid remain unanswered. Results from previous X-ray absorption fine structure (EXAFS) studies of both Me–Co^{3+}CFeSP and Co^{2+}CFeSP suggested that, in each case, the enzyme-bound corrinoid lacks a lower axial ligand, thus adopting an unprecedented five-coordinate and four-coordinate Co-coordination environment, respectively.[16,17]

However, this hypothesis appears to be inconsistent with the published EPR spectrum of Co^{2+}CFeSP,[12] which is interpreted as indicating the presence of an oxygen-based ligand (vide infra) in one of the axial positions of the cobalt center. Nonetheless, a subsequent detailed analysis of the pre-edge features in the X-ray absorption (XAS) spectrum of the Co^{2+}CFeSP continued to suggest that the Co^{2+}corrinoid cofactor exists in an unprecedented four-coordinate square-planar geometry.[16,18]

Numerous thermodynamic studies of alkylated corrinoid model complexes have shown that the nature of the lower ligand has a considerable influence on both the mode (i.e., homolytic vs heterolytic) and the rate of Co–C bond cleavage.[19-23] Consequently, the lower axial ligand is expected to play a key role in controlling both the reaction of Co^{1+}CFeSP with CH_3–H_4folate and the transfer of the methyl cation from Me–Co^{3+}CFeSP to the ACS A-cluster, and

it is therefore of considerable interest to unambiguously establish the binding scheme of the corrinoid cofactor in CFeSP. To this end, we have employed our recently developed combined spectroscopic and computational methodology[24-27] to probe the electronic structures, and thus indirectly the axial ligand interactions, of the methylated and Co^{2+}-containing forms of Factor III_m in the CFeSP active site.

Experimental

Purification of the CFeSP and Sample Preparation

The CFeSP from *Moorella thermoacetica* was purified to >95% homogeneity inside an anaerobic chamber (Vacuum Atmospheres, Hawthorne, CA), at an oxygen level of less than 2 ppm at 18 °C, according to a previously published procedure.[12] Me–Co^{3+}CFeSP was prepared by reducing as-isolated CFeSP with 5 equiv of titanium citrate per mol of enzyme and subsequently adding 2–3 equiv of methyl iodide. After incubation at 55 °C for ~10 min, the samples were allowed to cool to room temperature. Conversion to the methylated product was confirmed by electronic absorption (Abs) spectroscopy. The extent of methylation was quantified by parallel radiolabeling studies using ^{14}C-labeled methyl iodide, which showed the incorporation of 1.0 methyl groups/heterodimer. All resulting protein solutions were concentrated for further spectroscopic studies using an Amicon filter equipped with a YM30 membrane.

Spectroscopy

Samples used for Abs, circular dichroism (CD), and magnetic CD (MCD) experiments were prepared by mixing suitably concentrated protein solutions (in 0.1 M TRIS/HCl, pH 7.60) with the glassing agent glycerol (45% v/v) and injecting the resulting mixtures into MCD cells that were then immediately frozen in liquid nitrogen. All 4.5 K Abs spectra obtained in this study were consistent with previously published room-temperature data, indicating that the addition of glycerol and subsequent freezing had negligible effects on the CFeSP-bound corrinoid cofactor. Sample concentrations ranged from 0.5 to 1.0 mM CFeSP and were determined spectrophotometrically at 300 K on the basis of published molar extinction coefficients (i.e., $\varepsilon_{470\ nm}$ = 13.2 mM^{-1} cm^{-1} for the Co^{2+}CFeSP and $\varepsilon_{450\ nm}$ = 12.5 mM^{-1} cm^{-1} for Me–Co CFeSP).[12] Adenosylcobinamide (AdoCbi$^+$) was prepared enzymatically as described previously.[28] Low-temperature Abs, CD, and MCD spectra were recorded using a JACSO J-715 spectropolarimeter in conjunction with an Oxford Instruments SM-4000 8T magnetocryostat. The MCD spectra reported herein were obtained by subtracting the −7 T spectrum from the +7 T spectrum to eliminate the natural CD contributions. Resonance Raman (rR) samples of H_3C-, ^2H_3C-, and $H_3^{13}C$-bound Me–Co^{3+}CFeSP were prepared as described above, using the correspondingly labeled methyl iodides. Aliquots of 10–15 μL of the resulting 2–3 mM Me–Co^{3+}CFeSP solution were loaded under anaerobic and reduced light conditions into sample cells consisting of 2 mm holes drilled into a 3 mm thick copper plate. The copper plate was attached to a coldfinger and inserted into a liquid nitrogen dewar that was then placed under vacuum to degas the sample and prevent frost formation. Samples of free base-off MeCbl were prepared by dissolving MeCbl (purchased from Sigma) in 0.1 M HCl, and the resulting solutions were loaded onto the coldfinger as described above for the enzyme sample. All rR spectra were accumulated upon excitation at 441.6 nm using a Liconix 4200 series He–Cd laser (model 4240NB) with ~16–18 mW laser power at the sample that was cooled to 77 K to inhibit laser induced Co–C bond photolysis. The scattered light was collected in an ~135° backscattering geometry and focused onto the slit of a Spex 1877 triple monochromator equipped with a 2400 groves/mm grating. A liquid nitrogen cooled charge coupled device (Spec-10 system, Princeton Instruments) with 1340 × 400 pixels was used as the multichannel detector. Raman shifts were calibrated using *N,N*-dimethylformamide as a standard loaded into an adjacent sample cell.

EPR spectra were recorded at 100 K using a Bruker EMX spectrometer (Billerica, MA) equipped with an X-band High Sensitivity resonator, an HP5352B frequency counter (Hewlett-Packard, Palo Alto, CA), and an ESR 900 continuous flow cryostat (Oxford, Billerica, MA). All other pertinent details for EPR data acquisition are provided in the caption of Figure 3. $Co^{2+}CFeSP$ EPR samples were prepared by concentrating ~120 nmol of protein, resuspending the pellet in 20 μL of 1 M potassium phosphate buffer pH = 7.8, and slowly adding 180 μL of either H_2O or H_2 ^{17}O. Total spin concentrations as determined by double integration of the 100 K spectra were found to be 0.40 mM and 0.44 mM for the H_2O and H_2 ^{17}O samples, respectively. The final level of H_2 ^{17}O enrichment was estimated to be 60% based on the dilution of water into the sample mixture. EPR data were simulated using the WEPR program written by Dr. Frank Neese. The parameter sets employed for these EPR simulations are given in the Supporting Information.

Computational Methods

The combined quantum mechanical/molecular mechanical (QM/MM) approach[29] was employed to generate corrinoid models that have been shown to accurately predict the corresponding geometric and electronic structures.[30] As no crystal structures have yet been reported for $Me–Co^{3+}CFeSP$ and free base-off MeCbl (as well as the closely related derivative methylcobinamide, $MeCbi^+$), an initial model of the enzyme-bound cofactor (Figure 1) was constructed on the basis of the high-resolution (0.8 Å) crystal structure data available for base-on MeCbl.[31] The nucleotide loop was cleaved at the phosphoester bond proximal to C^{17}, and the remaining distal loop fragment was deleted. A water molecule was substituted for the DMB base in the lower axial position, and the geometry of the entire model was optimized using the QM/MM method[32,33] as implemented in the Amsterdam Density Functional (ADF) 2004.01 suite of programs.[34-36] Only those atoms that were expected to have a significant *electronic* influence on the geometry of this $MeCbi^+$ model were treated at the QM level; namely, the cobalt center, both axial ligands (H_2O and CH_3), and all atoms that comprise the corrin macrocycle. The computational treatment of this QM region employed the Vosko–Wilk–Nusair local density approximation (VWN-LDA)[37] and the gradient corrections of Becke[38] and Perdew[39] for exchange and correlation, respectively, along with the ADF IV basis set (triple ζ with polarization on all heavy atoms). Alternatively, the atoms of the corrin ring substituents that have merely *steric/electrostatic* influences on the cofactor geometry were treated at the MM level using the Amber 95 force field[40] and were coupled to the QM region using the multipole derived charge analysis model as implemented in ADF.[41] QM/MM geometries were updated using the BFGS Hessian scheme in optimizations carried out with an integration constant of 4.0 on a cluster of Pentium Xeon processors (ACE Computers).

Using this optimized model as a starting geometry, the effects of lower ligand distortions on the geometric structure of $MeCbi^+$ were examined by varying the Co–O bond length in fixed increments of 0.1 Å between 1.800 and 3.000 Å and reoptimizing the positions of all remaining atoms using the QM/MM method described above. The effects of these distortions on the predicted ground and excited-state electronic properties were investigated by density functional theory (DFT) and time-dependent DFT (TD-DFT) calculations, which were carried out on a desktop PC using the ORCA 2.2 software package developed by Dr. Frank Neese (MPI Mülheim, Germany).[42] As the QM/MM optimized models of $MeCbi^+$ were too large for computations based entirely on DFT, the corresponding QM region of each model was excised and used as-is for all subsequent calculations. Ground-state DFT calculations employed Becke's three-parameter hybrid functional for exchange[43,44] combined with the Lee–Yang–Parr correlation functional[45] (B3LYP/G) using the default 20% Hartree–Fock exchange. All atoms were treated with the SV(P) (Ahlrichs polarized split valence) basis[46] in conjunction with the SV/C auxiliary basis with the exception of the Co center for which the TZVP triple-ζ basis was used.[47] Electronic transition energies and intensities for all models were computed

by the TD-DFT method[48-50] within the Tamm–Dancoff approximation[51,52] as implemented in ORCA 2.2, using the same functional and basis sets described above for the ground-state calculations. In each case, 60 excited states were computed by including all one-electron excitations between molecular orbitals within ±3 hartrees of zero energy. To increase computational efficiency, the resolution of the identity approximation was employed in calculating the Coulomb term.[53] The TD-DFT results were then used to simulate Abs spectra assuming that each electronic transition gives rise to a Gaussian-shaped band with a full width at half-maximum of $\nu_{1/2} = 1250$ cm^{-1}. Under this assumption, the molar extinction coefficient ε_{max} (M^{-1} cm^{-1}) is related to the TD-DFT predicted oscillator strength f according to the formula $f = 4.61 \times 10^{-9} \varepsilon_{max} \nu_{1/2}$.[54] All spectra were red-shifted by 3000 cm^{-1} to compensate for the fact that transition energies for Co^{3+}-corrinoids and similar systems are consistently overestimated by the B3LYP TD-DFT method.[24-27,49,53,55-57]

Results and Analysis

Spectroscopic Studies. (i) Abs, CD, and MCD Spectra of Co^{2+}CFeSP

The 4.5 K electronic absorption (Abs) spectrum of as-isolated CFeSP (Co^{2+}CFeSP) is presented in Figure 2 along with that of free Co^{2+}cobinamide (Co^{2+}Cbi$^+$), a cobalamin derivative that lacks the nucleotide base and consequently coordinates a water molecule in the lower axial position.[25,58,59] Both spectra exhibit a broad feature in the visible region with an absorption maximum at 470 nm (21,200 cm^{-1}); however, the Co^{2+}CFeSP spectrum possesses additional intensity near 420 nm (23,800 cm^{-1}) that we attribute to S→Fe^{3+} charge-transfer transitions from the oxidized [Fe$_4$S$_4$] cluster present in this sample. In support of this assignment, taking the difference of the two Abs spectra presented in Figure 2 yields a trace (Figure S1) that is very similar to the Abs spectrum reported for the [Fe$_4$S$_4$]$^{2+}$ component of CFeSP lacking the corrinoid cofactor.[12] The Abs feature at 470 nm, termed the α-band, has been shown to arise from the lowest-energy corrin-based π→π* (cor π→π*) transition. Past spectroscopic and computational studies have shown that the energy of this band is quite sensitive to the nature of the axial ligand found in Co^{2+}corrinoids.[25] Hence the fact that the α-band in the spectra of the CFeSP-bound corrinoid and free Co^{2+}Cbi$^+$ appears at precisely the same energy precludes any significant differences in axial ligand bonding interactions between the free and enzyme-bound cofactors.

The 4.5 K CD spectrum of Co^{2+}CFeSP contains features at 13,750, 15,900, 22,450, and 23,350 cm^{-1} that have no counterparts in the free Co^{2+}Cbi$^+$ spectrum, suggesting that they arise from the oxidized [Fe$_4$S$_4$] cluster. Intriguingly, the positions and relative intensities of these CD bands do not follow the spectral pattern typically observed for the [Fe$_4$S$_4$]$^{2+}$ state of ferredoxin-type or high-potential [FeS] clusters.[60] This difference perhaps reflects the necessity of the [Fe$_4$S$_4$] cluster of CFeSP to possess a somewhat unique electronic structure as judged on the basis of the unusually low midpoint potential of –523 mV versus SHE.[13]

While both the Abs and CD spectroscopic data of the Co^{2+}CFeSP presented above contain significant contributions from the diamagnetic [Fe$_4$S$_4$]$^{2+}$ cluster, the corresponding 4.5 K 7 T MCD spectrum should be dominated entirely by the corrinoid features due to the dramatic enhancement of MCD C-terms arising from paramagnetic species at low temperatures. Indeed, all features in the Co^{2+}CFeSP MCD spectrum (Figure 2) were found to decrease in intensity with increasing temperature as predicted for an $S = {}^1/_2$ species. Inspection of Figure 2 reveals that, although the Co^{2+}CFeSP MCD spectrum is quite similar to the free Co^{2+}Cbi$^+$ spectrum, some notable differences occur in the low energy region (<20,000 cm^{-1}) where Co^{2+} d→d transitions produce the dominant spectral contributions. In particular, two broad temperature-dependent features centered at 13,000 and 14,700 cm^{-1} are exclusive to the spectrum of the as-isolated enzyme. However, MCD data of the reduced [Fe$_4$S$_4$] ferredoxin from *Clostridium pasteurianum* exhibit a strikingly similar pattern of features at 13,500 and 15,000 cm^{-1} (as

well as 19,000 cm^{-1}),[61] suggesting that all the major differences between the two MCD spectra shown in Figure 2 are due to the presence of a small fraction of $[Fe_4S_4]^{1+}$ cluster in the protein sample. Nonetheless, a quantitative spectral analysis of the Co^{2+}CFeSP MCD data revealed that minor shifts do occur for some of the Co^{2+} d→d transitions (see Table 1) from their positions determined for free $Co^{2+}Cbi^+$ by a simultaneous Gaussian deconvolution of the Abs, CD, and MCD spectra.[25] This perturbation of the relative energies of the Co^{2+} d-based MOs is intriguing but not necessarily unexpected, as the $Co^{2+/1+}$ reduction potential of the free $Co^{2+}Cbi^+$ is ~14 mV more positive than that of the CFeSP-bound corrinoid. In fact, the relatively small shifts observed for some Co^{2+} d→d transitions (e.g., 150 cm^{-1} for band 1, Table 1) in response to cofactor binding to the enzyme active site likely reflects a slight destabilization of the Co^{2+} d_{z^2}-based redox active orbital and thus a minor depression of the $Co^{2+/1+}$ reduction potential. Ultimately, however, the close resemblance of the two data sets in Figure 2 precludes any significant differences between the Co^{2+} ligand environments in $Co^{2+}Cbi^+$ and Co^{2+}CFeSP.

EPR Studies of Co^{2+}CFeSP

The X-band EPR spectrum of Co^{2+}CFeSP in natural abundance H_2O (Figure 3, top) is essentially identical to that previously reported by Ragsdale and co-workers.[12] The pattern of eight negative resonances centered at $g_\parallel = 2.0$ and split by 144 G results from the unpaired electron localized in the Co $3d_{z^2}$-based orbital interacting with the spin of the ^{59}Co nucleus ($I = ^7/_2$).[62,63] The lack of any additional fine structure due to coupling from a ^{14}N nucleus ($I = 1$) confirms that the CFeSP-bound cofactor exists in the base-off conformation where the MBI ligand is dissociated, thus opening a potential coordination site for either a solvent molecule or a CFeSP-active site residue. Parallel experiments using Co^{2+}CFeSP resuspended in H_2 ^{17}O enriched buffer yielded an EPR spectrum suffering from significant broadening and an ~60% decrease in intensity throughout the $g_\parallel$ region (2800–4000 G) compared to the spectrum obtained in H_2 ^{16}O (Figure 3). This dramatic loss of intensity correlates almost exactly to the level of H_2 ^{17}O enrichment (60%, see Experimental Section) and, thus, must be attributed to spectral broadening induced by the strong superhyperfine coupling of the electron spin to the ^{17}O ($I = ^5/_2$) nucleus of a water molecule bound to the Co^{2+} center. Although simulation of the natural abundance Co^{2+}CFeSP spectrum (Figure 3, top) required slightly larger ^{59}Co hyperfine values A_i (^{59}Co) compared to those reported for free $Co^{2+}Cbi^+$,[27] overall, the EPR parameters for the free and enzyme-bound cofactors are quite similar (Table 2). The spectrum obtained in H_2 ^{17}O was fit assuming a 40% contribution from the H_2 ^{16}O spectrum described above. The remaining spectral intensity was simulated using ^{17}O hyperfine tensor elements A_i (^{17}O) set to values calculated by the coupled-perturbed SCF DFT method for a $Co^{2+}Cbi^+$ model described in our earlier work[25] (see Supporting Information for computational details). This treatment resulted in an excellent reproduction of the different intensity distribution within the labeled and unlabeled spectra and an accurate prediction of the fine structure caused by superhyperfine coupling to the ^{17}O nucleus (Figure 3).

Abs, CD, and MCD Spectra of Me–Co^{3+}CFeSP

Similar to the case of Co^{2+}CFeSP, the electronic Abs spectrum of the CFeSP containing the methylated corrinoid cofactor (Me–Co^{3+}CFeSP) is dominated by a broad feature in the visible region that, in this case, is reminiscent of the α-band in the Abs spectrum of free adenosylcobinamide (AdoCbi$^+$, Figure 4).[24] The appearance of this band at 450 nm (22,200 cm^{-1}) in the protein spectrum eliminates the possibility that the methoxybenzimidazolyl (MBI) moiety of Factor III$_m$ directly coordinates to the cobalt center, as the α-bands of alkylated corrinoids with N-donor ligands in the lower axial position consistently peak between 535 and 515 nm (18,700–19,500 cm^{-1}). While this result suggests that the MBI ligand is displaced by a water molecule in the enzyme-bound cofactor, the α-band in the Me–Co^{3+}CFeSP Abs spectrum is blue-shifted by 8 nm (390 cm^{-1}) relative to that of free AdoCbi$^+$ (Figure 4),

signaling, perhaps, a previously unknown mode of cofactor binding. The origin of this blue shift is addressed below in the Computational Studies section. The remaining spectral differences between the Abs spectra of Me–Co^{3+}CFeSP and AdoCbi$^+$ can be ascribed to contributions from the oxidized [Fe$_4$S$_4$]$^{2+}$ cluster to the former, as the single intense feature in the difference spectrum is a broad band centered at 420 nm (Figure S2).

The CD spectra of Me–Co^{3+}CFeSP and AdoCbi$^+$ (Figure 4, middle) are quite similar in that both exhibit a prominent positively signed feature at 330 nm (30,300 cm^{-1}). Removing the contributions from the methylated corrinoid via the same subtraction procedure employed for the Abs spectra yields a CD spectrum with features at 13,500, 15,800, 17,800, and 23,400 cm^{-1}, which line up almost exactly with the series of peaks observed in the difference CD spectrum between Co^{2+}CFeSP and Co^{2+}Cbi$^+$ described above. This high degree of similarity provides further support for our assumption that these four features arise from the [Fe$_4$S$_4$]$^{2+}$ cluster. The fact that the positions of all four features are identical (within experimental error) in the two difference spectra indicates that the electronic properties of the [Fe$_4$S$_4$]$^{2+}$ cluster do not depend on the Co oxidation state, consistent with previous potentiometric studies.[13]

As both the methylated Factor III$_m$ and the oxidized [Fe$_4$S$_4$]$^{2+}$ cluster are diamagnetic, the MCD spectral intensity of Me–Co^{3+}CFeSP should be temperature-independent. However, the corresponding MCD spectrum obtained at 7 T actually exhibited temperature-dependent features attributed to a minor fraction of reduced Co^{2+}CFeSP (cf. Figures S4 and 2). Yet, by elevating the temperature to 100 K, the contributions from this paramagnetic impurity could be eliminated, yielding an MCD spectrum similar to that of free AdoCbi$^+$ with respect to the relative intensities and energies of the dominant features (Figure 4, bottom). Note that the contributions from the [Fe$_4$S$_4$]$^{2+}$ cluster to the MCD spectrum of Me–Co^{3+}CFeSP should be insignificant, as they are expected to be ~50-fold less intense than MCD features associated with the Co^{3+} form of the corrinoid.[61]

Resonance Raman Data of Me–Co^{3+}CFeSP

The visible region of the Abs spectrum of Me–Co^{3+}CFeSP has contributions from both the corrinoid and the oxidized [Fe$_4$S$_4$]$^{2+}$ cluster (vide supra); therefore, laser excitation near the center of this Abs envelope is expected to give rise to resonance Raman enhancement of vibrational features from both cofactors. In Figure 5, the low-frequency region of the resonance Raman (rR) spectra obtained with 441.6 nm laser excitation of Me–Co^{3+}CFeSP samples are compared to that of base-off MeCbl (pH = 1). Isotopic labeling of the axial methyl group of free base-off MeCbl has previously been used to identify the Co–C stretching (ν_{Co-C}) mode as the peak appearing at 501 cm^{-1} (Figure 5A).[64] To determine if ν_{Co-C} also corresponds to the 501 cm^{-1} feature in the rR spectrum of natural abundance Me–Co^{3+}CFeSP (Figure 5B) we have isotopically labeled the enzyme-bound cofactor. Indeed, selective ^{13}C labeling of the methyl group downshifts the ν_{Co-C} mode by 10 cm$^-$ to 491 cm^{-1} (Figure 5C); it shifts further, to 480 cm^{-1}, when the methyl group is fully deuterated (Figure 5D). As the frequency of the ν_{Co-C} mode and the magnitudes of the isotope shifts for Me–Co^{3+}CFeSP are identical to those observed for base-off MeCbl,[64] it can be concluded that the Co–C bond strength is unaffected by binding of the cofactor to the protein. Moreover, the high-energy region of the spectrum, which is dominated by corrin-based modes, is also nearly identical for base-off MeCbl and Me–Co^{3+}CFeSP (cf. Figure 5A, D). This finding provides an interesting contrast to the situation encountered for B$_{12}$-dependent methylmalonyl-CoA mutase (MMCM), where rR data revealed a significant frequency upshift by ~4 cm^{-1} of corrin ring modes upon binding of the adenosylcobalamin cofactor to the enzyme active site.[65] In the case of MMCM, this perturbation of the corrin modes was interpreted as indicating that the enzyme active site forces the macrocycle to adopt a more planar conformation.

While MCD data yield little insight into the geometric and electronic properties of diamagnetic $[Fe_4S_4]^{2+}$ clusters, rR spectroscopy has proven to be an extremely powerful tool for identifying the set of endogenous ligands that coordinate the iron atoms of the protein-bound cluster. In the rR spectrum of Me–Co^{3+}CFeSP, a series of four peaks at 333, 340, 355, and 380 cm^{-1} are evident that have no counterparts in the spectrum of free base-off MeCbl and, therefore, can be attributed to the oxidized $[Fe_4S_4]^{2+}$ cluster. Based on its large intensity, the 333 cm^{-1} peak is assigned to the totally symmetric breathing mode of the FeS core; it falls within the range of frequencies (333–339 cm^{-1}) reported for $[Fe_4S_4]^{2+}$ clusters with all cysteinyl coordination. While only three cysteines have thus far conclusively been shown to coordinate to the $[Fe_4S_4]$ cluster in CFeSP, five Cys residues are actually present in the protein sequence of the 48 kDa subunit, making all-cysteinyl ligation of this cluster possible.[9]

Computational Studies. (i) Bonding Descriptions

Previously, it has been shown that the nature of the axial ligand set has a large influence on the appearance of the Abs spectrum of Co^{3+}corrinoids.[24,66-68] Further exploration of this spectral/structural relationship using TD-DFT calculations allowed us to correlate spectral changes observed upon MeCbl binding to MMCM to specific molecular distortions of the corrinoid cofactor.[26] In the current study, we employed a similar approach to explore the structural origin of the spectroscopic differences between free AdoCbi$^+$ and Me–Co^{3+}CFeSP described above. As no X-ray crystal structure exists for the methylated Factor III$_m$ bound to CFeSP, a model of this cofactor (including the full complement of corrin ring substituents) was constructed using the combined quantum mechanics/molecular mechanics (QM/MM) methodology (see Computational Methods for details). Importantly, this computational scheme explicitly accounts for all electrostatic and steric effects imposed by the peripheral ring substituents on the corrin ring. The lowest energy structure, assumed to reflect the equilibrium geometry of the free MeCbi$^+$, possessed a Co–OH$_2$ bond length of 2.250 Å. By varying this lower ligand bond length in fixed increments of 0.1 Å between 1.8 and 3.0 Å and minimizing the computed total energy with respect to the positions of all other atoms, a series of models were generated that represent points along the lower ligand dissociation coordinate. The potential energy surface associated with this axial ligand bond elongation, obtained by plotting the SCF energy of the QM region versus the Co–OH$_2$ bond length (Figure 6A), exhibits a very shallow, broad minimum and reveals that <4 kcal/mol are required to completely dissociate the water ligand. As the Co–OH$_2$ bond is lengthened, the Co–O σ-bonding interaction is weakened and the bond order decreases in a monotonic fashion (Figure 6C). Concomitant with this reduction in Co–O bond strength, all MOs that possess significant Co^{3+} 3d$_{z^2}$-orbital character are stabilized in energy due to a decrease in the Co–O σ-antibonding interaction induced by the strongly electron-donating methyl group trans to the water ligand (Figure 7).[24] Most importantly, however, the effect of this axial Co–OH$_2$ bond elongation on the Co–C bonding coordinate is almost negligible; the Co–C bond length is predicted to change by no more than 0.01 Å (Figure 6B) and the bond order, by <3% over the entire range of Co–OH$_2$ bond lengths investigated (Figure 6C). A similarly weak response of the Co–C bond properties to lower ligand distortion has been observed in previous computations for base-on MeCbl.[26,64,69,70] This lack of a significant trans influence is readily understood upon inspection of the qualitative axial ligand MO diagram in Figure 7, which reveals that even complete loss of the water ligand should not affect the Co–C bond order (this prediction is fully consistent with the conclusion drawn from our earlier work on Me–Co^{3+}corrinoids possessing different lower ligands).[24] Collectively, these results indicate that the nature of the Co–C bond is insignificantly affected by changes in the trans axial ligand position and/or identity; thus, protein induced distortions at the lower face of the corrinoid are not expected to affect the strength of the Co–C bond to any significant degree.

Spectro/Structural Correlation

The effects of axial ligand bond deformations on the appearance of the electronic Abs spectrum of corrinoids can be explored computationally using the TD-DFT method as demonstrated recently by Brooks et al.[26] TD-DFT computed Abs spectra for selected MeCbi$^+$ models that represent points along the lower ligand dissociation coordinate (Figure 6) are shown in Figure 8. These spectra reveal that the position of the intense α-band that dominates the visible region of the computed (and experimental) MeCbi$^+$ Abs spectrum is particularly sensitive to variations in the Co–OH$_2$ bond length. This sensitivity reflects the small but significant Co 3d$_{z^2}$-orbital character (~5%) carried by the HOMO that serves as the donor MO in the transition responsible for the α-band (Figure 7). As the lower ligand bond length increases, the consequent weakening of the Co–O σ-antibonding interaction leads to stabilization of the HOMO and, thus, to an increase in the energy of the α-band transition. Our TD-DFT results predict that the α-band blue-shifts by ~20 cm^{-1}/pm as the Co–OH$_2$ bond is lengthened from its equilibrium position toward the dissociation limit (Table S8).[71] Therefore, a 0.2 Å increase in the Co–OH$_2$ bond length is sufficient to rationalize the 390 cm^{-1} blue-shift of the α-band observed experimentally when comparing AdoCbi$^+$ to Me–Co^{3+}CFeSP (Figure 4A). Note that for a Co–OH$_2$ bond length change of this magnitude, the positions of the higher-energy Abs features are predicted to be virtually unaffected (Figure 8), consistent with our CD data of AdoCbi$^+$ and Me–Co^{3+}CFeSP (Figure 4B). Importantly, elongation of the Co–OH$_2$ bond beyond 2.5 Å or complete removal of the lower ligand results in changes in the predicted Abs spectrum that are too dramatic to be consistent with our experimental data. Therefore, it is reasonable to conclude that, like free MeCbi$^+$ and AdoCbi$^+$, the Me–Co^{3+}CFeSP maintains a water ligand in the lower axial position; however the Co^{3+}–O bond length is slightly lengthened for the protein-bound cofactor.[72]

Discussion

The biogenesis of acetyl-CoA is an essential step in the Wood–Ljungdahl pathway for energy generation and/or carbon fixation by a variety of anaerobic microbes. While it has been known for some time that the methyl group required for this reaction is supplied to the active site of acetyl-CoA synthase (ACS) by a corrinoid-iron–sulfur protein (CFeSP), the nature of the coordination environment of the corrinoid cofactor in the physiologically relevant Co^{3+} and Co^{2+} oxidation states has remained the subject of some debate. This is an important issue because axial ligation can markedly influence the mechanism and the rate of methyl transfer and the efficiency and rate of reduction of inactive Co^{2+} to the active Co^{1+} state.[19-23,73,74] To better understand the nature of axial coordination, we have compared the MCD, EPR, and resonance Raman spectra of the free corrinoid center with those of CFeSP-bound Factor III$_m$. Using our earlier spectroscopic characterizations of free AdoCbi$^+$ and Co^{2+}Cbi$^+$ as the basis for a comparison,[24,25] we have evaluated spectral differences observed between these free corrinoids and the methylated and reduced forms of the CFeSP-bound 5-methoxybenzimidazolyl cobamide cofactor (Factor III$_m$) in terms of enzyme-induced perturbations of the lower axial ligand. The implications of our findings with respect to the mechanisms of Co^{2+}CFeSP reactivation and methyl group transfer from Me–Co^{3+}CFeSP to ACS are discussed below.

Reactivation of Co^{2+}CFeSP

Based on the close resemblance of the corresponding MCD spectra, we conclude that the corrinoid cofactor present in as-isolated, oxidatively inactivated Co^{2+}CFeSP experiences a nearly identical coordination environment as free Co^{2+}Cbi$^+$ (Figure 2); namely, it is bound in the base-off conformation where the lower methoxybenzimidazolyl (MBI) moiety is displaced and a water molecule or a protein-derived oxygen-donor ligand binds to the cobalt center. Further insight into the axial ligation of Factor III$_m$ in CFeSP is provided by the EPR spectrum

of Co^{2+}CFeSP obtained in isotopically labeled water (Figure 3). The dramatic loss of intensity in the $g_\parallel$ region of this spectrum relative to the spectrum in natural abundance water is readily attributed to ^{17}O-induced hyperfine broadening and conclusively proves that H_2O coordinates to the metal center in one of the open axial positions.

Originally, the appearance of a modestly intense pre-edge ($1s \rightarrow 3d$) feature in X-ray Abs spectra of Co^{2+}CFeSP had been interpreted as indicating that the cobalt ion in the enzyme-bound cofactor occupies a near-centrosymmetric site, consistent with an approximately four-coordinate square-planar ligand environment.[16,17] Yet, on the basis of our recent computational studies on a series of $Co^{2+}Cbi^+$ models with varying $Co–OH_2$ bond lengths, lower axial ligand dissociation should drastically alter the energies of the Co 3d-based ligand field (LF) transitions and the EPR parameters (e.g., g-values and ^{59}Co hyperfine coupling constants).[27] However, no such dramatic alterations are actually observed in the case of as-isolated Co^{2+}CFeSP, thus arguing against the presence of a four-coordinate Co^{2+}corrinoid species in this enzyme. Further evidence against this unusual Co^{2+} ligand environment proposed for Co^{2+}CFeSP comes from our recent studies of Co^{2+}Cbl bound to the human methionine adenosyltransferase (ATR), which permitted the first spectroscopic characterization of a four-coordinate Co^{2+}corrinoid species.[75] As predicted by our computations, the spectral properties of this species were found to be strikingly different from those of either $Co^{2+}Cbi^+$ or Co^{2+}CFeSP.

ATRs involved in adenosylcobalamin biosynthesis and corrinoid-dependent methyltransferases (e.g., methionine synthase (MetH) and the CFeSP) are thought to employ a common mechanism for Co–C bond formation wherein the metal center of the corrinoid substrate is fully reduced to form a four-coordinate Co^{1+} supernucleophile that is able to attack the target carbon atom of the cosubstrate.[75-78] Owing to the low reduction potential of the $Co^{2+/1+}$ couple, the Co^{1+} corrinoid intermediate is thermodynamically difficult to generate and vulnerable to oxidative inactivation back to the Co^{2+} state. To achieve and maintain the Co^{1+} oxidation state, human ATR forces the Co^{2+}corrinoid substrate into a four-coordinate conformation, which helps to lower the thermodynamic barrier for cobalt-ion reduction ($E° = -490$ mV for the $Co^{2+/1+}$ couple of $Co^{2+}Cbi^+$) by the in vivo flavodoxin reductant ($E° = -285$ mV).[74] CFeSP instead employs a low-potential $[Fe_4S_4]$ cluster ($E° = -523$ mV) as an internal reducing system that is bound to the enzyme through four cysteine residues,[14,15] as further indicated by our resonance Raman (rR) data (Figure 5). This $[Fe_4S_4]^{2+/1+}$ potential is intermediate between that of the C cluster of CODH (-530 mV)[79] and the $Co^{2+/1+}$ couple of the bound Factor III_m (-504 mV).[13] Therefore, it has been postulated that reductive activation begins with the CO-dependent reduction of the CODH C cluster that then transfers an electron to the $[Fe_4S_4]^{2+}$ cluster of the CFeSP, which reduces the bound Factor III_m to the Co^{1+} state.[14,15,80]

Reduction activation is enhanced by replacement of the lower axial MBI ligand of Factor III_m by a weaker water ligand when the cofactor binds to the CFeSP, generating a five-coordinate Co^{2+} species that resembles $Co^{2+}Cbi^+$ (see above). This ligand switch has a profound influence in the redox properties of the Co center, increasing the $Co^{2+/1+}$ reduction potential by ~120 mV relative to that of the MBI-bound form of the cofactor found in solution (~-620 mV).[13] Therefore, there is no thermodynamic barrier to corrinoid reduction, and CFeSP has no need to further stabilize the redox-active orbital of the Co^{2+} center via complete dissociation of the lower ligand, contrasting the situation encountered for ATRs.

Methyl Group Transfer from Me–Co^{3+}CFeSP to the ACS A-Cluster

Once the oxidatively inactivated Co^{2+}CFeSP is reduced to the Co^{1+} state by the $[Fe_4S_4]^{1+}$ cluster, a methyltransferase (MeTr) transfers a methyl cation from CH_3–H_4folate to the Co^{1+} corrinoid intermediate.[81] The product Me–Co^{3+}CFeSP then transfers this methyl group to the

A-cluster of ACS, generating what is believed to be a Ni–CH$_3$ intermediate. Kinetic experiments have shown that this transmethylation is reversible at low reduction potentials,[82] slightly favoring formation of the Ni–CH$_3$ species ($K_{eq} \approx 2.3$).[83] This result signifies that the Ni site of the A-cluster is at least as nucleophilic as the CFeSP-bound Co^{1+}corrinoid species. Recent computational studies performed in our laboratory established that the proposed Ni–CH$_3$ and Co–CH$_3$ bonds are similarly strong (with M–CH$_3$ stretching force constants of 1.76 and 1.84 mdyn/Å, respectively), an intuitive requirement for the reversibility of the methylation.[84] This computational study also indicated that the conformational flexibility of the Ni site in ACS likely plays a significant role in promoting formation of the Ni–CH$_3$ bond. Thus, while the structural features of the A-cluster, which facilitate Ni–CH$_3$ bond formation, are becoming increasingly well understood, the mechanism by which CFeSP tunes the reactivity of its Me–Co^{3+}corrinoid cofactor toward methyl-group transfer remained largely unknown. To explore possible perturbations of the methylated corrinoid's Co–C bond induced by CFeSP, we have compared spectroscopic data of Me–Co^{3+}CFeSP to those of free base-off MeCbl and AdoCbi$^+$, which are considered to be good spectroscopic models of the bound cofactor.[64,85] Indeed, the corresponding sets of electronic spectra are quite similar (Figure 4), suggesting that, as in Co^{2+}CFeSP, the MBI base that serves as the lower axial ligand in the free cofactor is displaced and a water molecule is instead coordinated in the enzyme-bound form. However, a noticeable blue-shift by 390 cm^{-1} of the α-band of Me–Co^{3+}CFeSP as compared to AdoCbi$^+$ suggests a slightly perturbed axial ligand bonding scheme. Conversely, rR spectra of the methylated enzyme indicate that the Co–C bond properties are not altered, as the frequency of the Co–C stretching mode is identical to that determined for base-off MeCbl (Figure 5). Likewise, the corrin-based modes (1400–1600 cm^{-1}, Figure 5) have exactly the same frequencies in the free and CFeSP-bound cofactor, ruling out any significant enzyme-induced perturbation of the corrin macrocycle. Therefore, we have engaged in TD-DFT calculations to analyze the spectral differences observed between the Abs spectra of Me–Co^{3+}CFeSP and base-off MeCbl in terms of an elongation of the Co–OH$_2$ bond (Figure 8). These computations attribute the 390 cm^{-1} blue-shift of the α-band to a 0.2 Å lengthening of the lower axial ligand bond. Importantly, however, lower ligand bond deformation is predicted to have a negligible effect on the trans axial Co–C bond (Figure 7), consistent with previous experimental studies that have shown ν$_{Co-C}$ to be virtually unaffected by axial ligand substitution and/or bond elongation.[24,64,70]

Currently, the motivation for this enzyme-induced Co–OH$_2$ bond lengthening with respect to the methyl group transfer mechanism is unclear. However, kinetic and thermodynamic studies of alkylated corrinoid species have shown that the nature of the lower ligand has a profound influence on the mode of Co–C bond breaking.[19,21,23] Specifically, the presence of an N-donor ligand in the lower axial ligand position inhibits heterolytic cleavage, whereas oxygen-donor ligands, such as water, show no such effect. This phenomenon is particularly well-exemplified by the ability of free MeCbi$^+$ to transfer its methyl group to ACS at a rate ~10^3 times faster than that of free MeCbl.[85] Intriguingly, Me-Co^{3+}CFeSP methylates ACS 100-fold faster than free MeCbi$^+$ does, signaling that the protein serves to provide additional driving force for this reaction. While some of this observed rate enhancement is certainly due to favorable protein–protein interactions between ACS and CFeSP, our spectroscopic and computational results suggest that enzyme-induced elongation of the lower axial ligand bond may also contribute. The computationally derived axial ligand bonding scheme presented in Figure 7 shows that lengthening the Co–OH$_2$ bond selectively stabilizes the formally unoccupied Co 3d$_{z^2}$ orbital so as to allow for increased mixing of this orbital with the corrin-based occupied frontier orbitals. Hence, elongation of the Co–OH$_2$ bond of the CFeSP-bound cofactor makes the cobalt center more "Co^{1+}-like", a requirement for facile heterolytic Co–C bond cleavage. Furthermore, by partially dissociating the lower water ligand, the enzyme also discourages homolytic bond cleavage given the strong preference of Co^{2+}corrinoids to retain an axial ligand. Moreover, the presence of a water molecule sequestered in the enzyme active site is

expected to lessen the kinetic barrier to methylation of the Co^{1+} intermediate. Thus, if the protein matrix can manipulate this Co–lower ligand interaction, e.g., through hydrogen bonding or direct involvement of an active site residue, then a mechanism for tuning the reversible methyl group transfer between CFeSP and ACS is easily imagined.

Supplementary Material

Refer to Web version on PubMed Central for supplementary material.

Acknowledgments

References

1. Ragsdale SW. Crit. Rev. Biochem. Mol. Biol 2004;39:165–195. [PubMed: 15596550]

2. Dobbek H, Svetlitchnyi V, Gremer L, Huber R, Meyer O. Science 2001;293:1281–1285. [PubMed: 11509720]

3. Darnault C, Volbeda A, Kim EJ, Legrand P, Vernede X, Lindahl PA, Fontecilla-Camps JC. Nature Structural Biology 2003;10:271–279.

4. Volbeda A, Fontecilla-Camps JC. J. Biol. Inorg. Chem 2004;9:525–532. [PubMed: 15221479]

5. Tan XS, Loke HK, Fitch S, Lindahl PA. J. Am. Chem. Soc 2005;127:5833–5839. [PubMed: 15839681]

6. Seravalli J, Kumar M, Ragsdale SW. Biochemistry 2002;41:1807–1819. [PubMed: 11827525]

7. Irion E, Ljungdahl LG. Biochemistry 1965;4:2780–2790. [PubMed: 5880686]

8. Ljungdahl LG, LeGall J, Lee J-P. Biochemistry 1973;12:1802–1808. [PubMed: 4699238]

9. Lu WP, Schiau I, Cunningham JR, Ragsdale SW. J. Biol. Chem 1993;268:5605–5614. [PubMed: 8449924]

10. Drennan CL, Matthews RG, Ludwig ML. Curr. Opin. Struct. Biol 1994;4:919–929. [PubMed: 7712296]

11. Although MBI is found in the native protein expressed by *M. thermoacetica*, when the CFeSP is reconstituted with cobalamin, its enzymatic properties are identical to those of the native protein (see ref [9]).

12. Ragsdale SW, Lindahl PA, Munck E. J. Biol. Chem 1987;262:14289–14297. [PubMed: 2821001]

13. Harder SR, Lu WP, Feinberg BA, Ragsdale SW. Biochemistry 1989;28:9080–9087. [PubMed: 2605242]

14. Menon S, Ragsdale SW. J. Biol. Chem 1999;274:11513–11518. [PubMed: 10206956]

15. Menon S, Ragsdale SW. Biochemistry 1998;37:5689–5698. [PubMed: 9548955]

16. Wirt MD, Kumar M, Ragsdale SW, Chance MR. J. Am. Chem. Soc 1993;115:2146–2150.

17. Wirt MD, Kumar M, Wu JJ, Scheuring EM, Ragsdale SW, Chance MR. Biochemistry 1995;34:5269–5273. [PubMed: 7711048]

18. Wirt MD, Sagi I, Chen E, Frisbie SM, Lee R, Chance MR. J. Am. Chem. Soc 1991;113:5299–5304.

19. Hogenkamp HPC, Rush JE, Swenson CA. The Journal of Biological Chemistry 1965;240:3641–3644. [PubMed: 5835943]

20. Hay BP, Finke RG. J. Am. Chem. Soc 1987;109:8012–8018.

21. Kräutler B. Helv. Chim. Acta 1987;70:1268–1278.

22. Garr CD, Sirovatka JM, Finke RG. J. Am. Chem. Soc 1996;118:11142–11154.

23. Pratt, JM. Chemistry and Biochemistry of B_{12}. Banerjee, R., editor. Wiley; New York: 1999. p. 73-112.

24. Stich TA, Brooks AJ, Buan NR, Brunold TC. J. Am. Chem. Soc 2003;125:5897–5914. [PubMed: 12733931]

25. Stich TA, Buan NR, Brunold TC. J. Am. Chem. Soc 2004;126:9735–9749. [PubMed: 15291577]

26. Brooks AJ, Vlasie M, Banerjee R, Brunold TC. J. Am. Chem. Soc 2004;126:8167–8180. [PubMed: 15225058]

27. Stich TA, Buan NR, Escalante-Semerena JC, Brunold TC. J. Am. Chem. Soc 2005;127:8710–8719. [PubMed: 15954777]

28. Suh S-J, Escalante-Semerena JC. J. Bacteriol 1995;177:921–925. [PubMed: 7860601]

29. Field MJ, Bash PA, Karplus M. Journal of Computational Chemistry 1990;11:700–733.

30. Personal communication with A. J. Brooks and T. C. Brunold.

31. Randaccio L, Furlan M, Geremia S, Slouf M, Srnova I, Toffoli D. Inorg. Chem 2000;39:3403–3413. [PubMed: 11196881]

32. Woo TK, Cavallo L, Ziegler T. Theor. Chem. Acc 1998;100:307–313.

33. Maseras F, Morokuma K. Journal of Computational Chemistry 1995;16:1170–1179.

34. te Velde G, Bickelhaupt FM, van Gisbergen SJA, Guerra CF, Baerends EJ, Snijders JG, Ziegler T. Journal of Computational Chemistry 2001;22:931–967.

35. Guerra CF, Snijders JG, te Velde G, Baerends EJ. Theor. Chem. Acc 1998;99:391–403.

36. ADF2004.01, SCM, Theoretical Chemistry. Vrije Universiteit; Amsterdam, The Netherlands: http://www.scm.com.

37. Vosko SH, Wilk L, Nusair M. Can. J. Phys 1980;58:1200–1211.

38. Becke AD. Physical Review A 1988;38:3098–3100. [PubMed: 9900728]

39. Perdew JP. Phys. Rev. B 1986;33:8822–8824.

40. Cornell WD, Cieplak P, Bayly CI, Gould IR, Merz KM Jr. Ferguson DM, Spellmeyer DC, Fox T, Caldwell JW, Kollman PA. J. Am. Chem. Soc 1995;117:5179–5197.

41. Swart M, Van Duijnen PT, Snijders JG. Journal of Computational Chemistry 2001;22:79–88.

42. Neese F, Solomon EI. Inorg. Chem 1999;38:1847–1865. [PubMed: 11670957]

43. Becke AD. J. Chem. Phys 1993;98:1372–1377.

44. Becke AD. J. Chem. Phys 1993;98:5648–5652.

45. Lee C, Yang W, Parr RG. Phys. Rev. B 1988;37:785–789.

46. Schäfer A, Horn H, Ahlrichs R. J. Chem. Phys 1992;97:2571–2577.

47. Schäfer A, Huber C, Ahlrichs R. J. Chem. Phys 1994;100:5829–5835.

48. Bauernschmitt R, Ahlrichs R. Chem. Phys. Lett 1996;256:454–464.

49. Casida EM, Jamorski C, Casida KC, Salahub DR. J. Chem. Phys 1998;108:4439–4449.

50. Stratmann RE, Scuseria GE, Frisch MJ. J. Chem. Phys 1998;109:8218–8224.

51. Hirata S, Head-Gordon M. Chem. Phys. Lett 1999;314:291–299.

52. Hirata S, Head-Gordon M. Chem. Phys. Lett 1999;302:375–382.

53. Neese F, Olbrich G. Chem. Phys. Lett 2002;362:170–178.

54. Lever, ABP. Inorganic Electronic Spectroscopy. Vol. 2nd ed. Elsevier; Amsterdam; New York: 1984.

55. Andruniow T, Kozlowski PM, Zgierski MZ. J. Chem. Phys 2001;115:7522–7533.

56. Craft JL, Horng YC, Ragsdale SW, Brunold TC. J. Biol. Inorg. Chem 2004;9:77–89. [PubMed: 14663648]

57. Craft JL, Horng YC, Ragsdale SW, Brunold TC. J. Am. Chem. Soc 2004;126:4068–4069. [PubMed: 15053571]

58. Van Doorslaer S, Jeschke G, Epel B, Goldfarb D, Eichel RA, Krautler B, Schweiger A. J. Am. Chem. Soc 2003;125:5915–5927. [PubMed: 12733932]

59. Giorgetti M, Ascone I, Berrettoni M, Conti P, Zamponi S, Marassi R. J. Biol. Inorg. Chem 2000;5:156–166. [PubMed: 10819461]

60. Stephens PJ, Thomson AJ, Dunn JBR, Keiderling TA, Rawlings J, Rao KK, Hall DO. Biochemistry 1978;17:4770–4778. [PubMed: 728385]

61. Johnson, MK.; Robinson, AE.; Thomson, AJ. Iron–Sulfur Proteins. Spiro, TG., editor. Wiley-Interscience; New York: 1982. p. 367-406.

62. Bayston JH, Looney FD, Pilbrow JR, Winfield ME. Biochemistry 1970;9:2164–2172. [PubMed: 4315132]

63. Pilbrow, JR. B$_{12}$. Dolphin, D., editor. Wiley; New York: 1982. p. 431-462.

64. Dong SL, Padmakumar R, Banerjee R, Spiro TG. J. Am. Chem. Soc 1996;118:9182–9183.

65. Dong SL, Padmakumar R, Maiti N, Banerjee R, Spiro TG. J. Am. Chem. Soc 1998;120:9947–9948.

66. Schrauzer GN, Lee L-P. J. Am. Chem. Soc 1968;90:6541–6543. [PubMed: 4300777]

67. Schneider, Z.; Stroinski, A. Comprehensive B$_{12}$: Chemistry, Biochemistry, Nutrition, Ecology and Medicine. De Gruyter; New York: 1987.

68. Pratt, JM. Chemistry and Biochemistry of B$_{12}$. Banerjee, R., editor. Wiley; New York: 1999. p. 113-164.

69. Kozlowski PM, Zgierski MZ. J. Phys. Chem. B 2004;108:14163–14170.

70. Dong SL, Padmakumar R, Banerjee R, Spiro TG. Inorg. Chim. Acta 1998;270:392–398.

71. While no experimental data are currently available to verify our TD-DFT based hypothesis that a lengthening of the Co–OH$_2$ bond in MeCbi$^+$ would give rise to a blue-shift of the α-band, we note that this prediction is consistent with the fact that substitution of the DMB in MeCbl (a moderately strong σ-donor) by a water ligand (a weak σ-donor) to generate MeCbi$^+$ gives rise to a substantial shift of the α-band in the Abs spectrum from ~18 950 to 21 800 cm^{-1} (see ref [24]). Hence, a further decrease in the σ-donor strength of the lower axial ligand, e.g., via lengthening of the Co−OH$_2$ bond, should give rise to an additional blue-shift of the α-band, consistent with our TD-DFT results.

72. (On the basis of a pressure-dependence study, van Eldik, Pratt, and co-workers (Hamza MSA, van Eldik R, Harper PLS, Pratt JM, Betterton EA. Eur. J. Inorg. Chem 2002:2580–2583.) proposed that the interconversion between the yellow (high-temperature) and red (low-temperature) forms of MeCbi$^+$ involves the coordination/release of a water molecule. However, their data do not provide any direct evidence that this putative additional water molecule in the red form occupies the lower axial position and that this position is vacant in the yellow form (which, spectroscopically, is indistinguishable from AdoCbi$^+$). In fact, on the basis of our TD-DFT based spectro/structural correlations (Figure 8), the close resemblance of the Abs spectra of the yellow and red forms of MeCbi$^+$, in particular the lack of any notable differences in the near-UV region, would suggest that the ligand environments of the Co^{3+} center in these two forms are actually quite similar.

73. Lexa D, Saveant J-M. J. Am. Chem. Soc 1980;102:4851–4852.

74. Lexa D, Saveant JM. Acc. Chem. Res 1983;16:235–243.

75. Stich TA, Yamanishi M, Banerjee R, Brunold TC. J. Am. Chem. Soc 2005;127:7660–7661. [PubMed: 15913339]

76. Banerjee RV, Harder SR, Ragsdale SW, Matthews RG. Biochemistry 1990;29:1129–1135. [PubMed: 2157485]

77. Fonseca MV, Escalante-Semerena JC. J. Biol. Chem 2001;276:32101–32108. [PubMed: 11408479]

78. Leal NA, Olteanu H, Banerjee R, Bobik TA. J. Biol. Chem 2004;279:47536–47542. [PubMed: 15347655]

79. Lindahl PA, Munck E, Ragsdale SW. J. Biol. Chem 1990;265:3873–3879. [PubMed: 2154491]

80. Tan XS, Sewell C, Yang QW, Lindahl PA. J. Am. Chem. Soc 2003;125:318–319. [PubMed: 12517128]

81. Doukov T, Seravalli J, Stezowski JJ, Ragsdale SV. Structure 2000;8:817–830. [PubMed: 10997901]

82. Lu WP, Harder SR, Ragsdale SW. J. Biol. Chem 1990;265:3124–3133. [PubMed: 2303444]

83. Tan XS, Sewell C, Lindahl PA. J. Am. Chem. Soc 2002;124:6277–6284. [PubMed: 12033855]

84. Schenker R, Mock MT, Kleber-Emmons MT, Riordan CG, Brunold TC. Inorg. Chem 2005;44:3605–3617. [PubMed: 15877445]

85. Seravalli J, Brown KL, Ragsdale SW. J. Am. Chem. Soc 2001;123:1786–1787. [PubMed: 11456791]
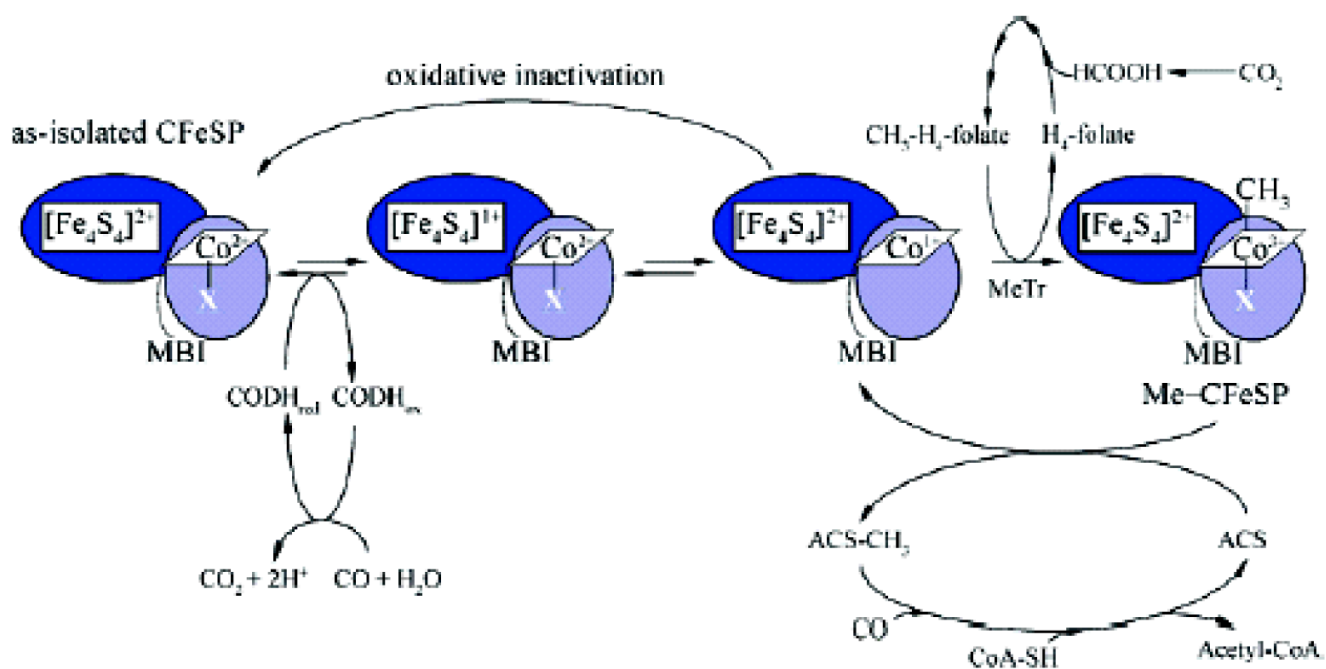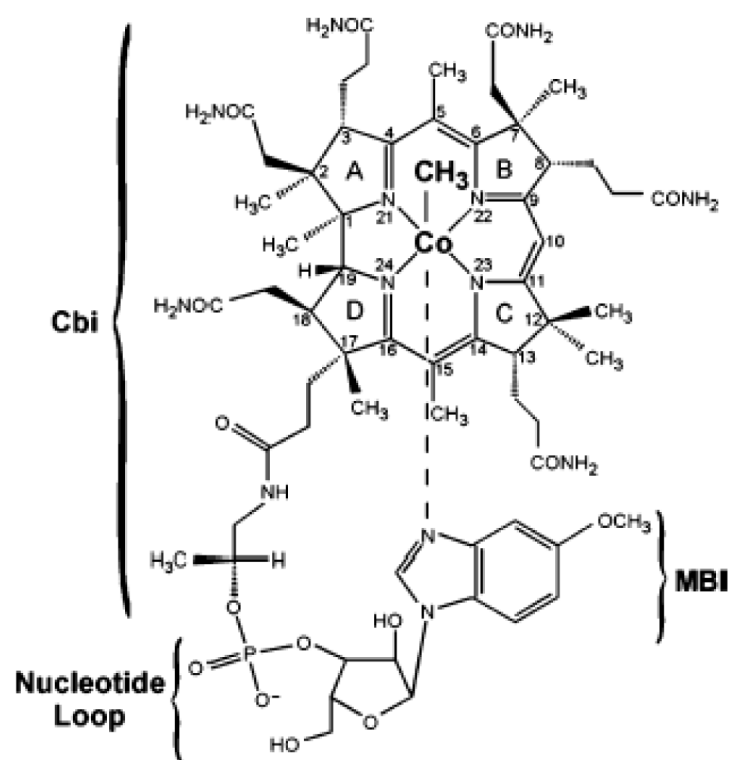
Scheme 1.
Adapted from ref [12].

Figure 1.
Chemical structure and numbering scheme for the CFeSP cofactor, Factor III_m (methyl-Co^{3+}–5′methoxybenzimidazolyl cobamide).
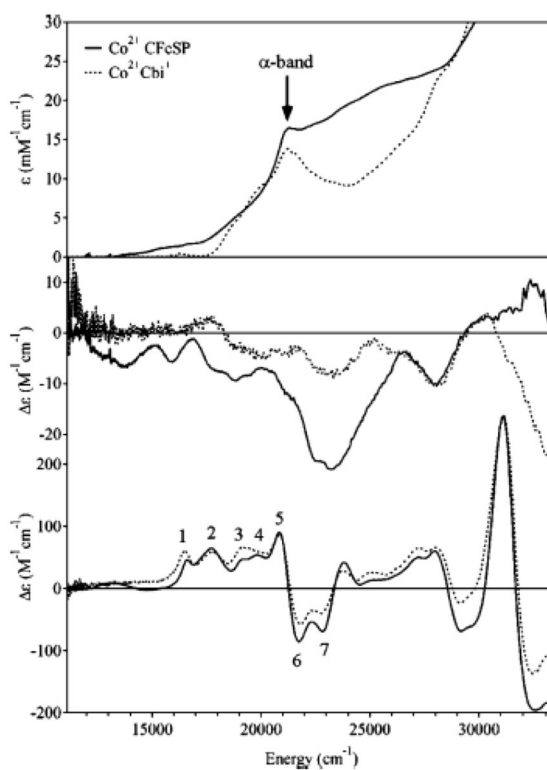
Figure 2.
Comparison of 4.5 K Abs (top), CD (middle), and 7 T MCD (bottom) spectra of as-isolated $Co^{2+}CFeSP$ (solid lines) and $Co^{2+}Cbi^+$ (dotted lines).
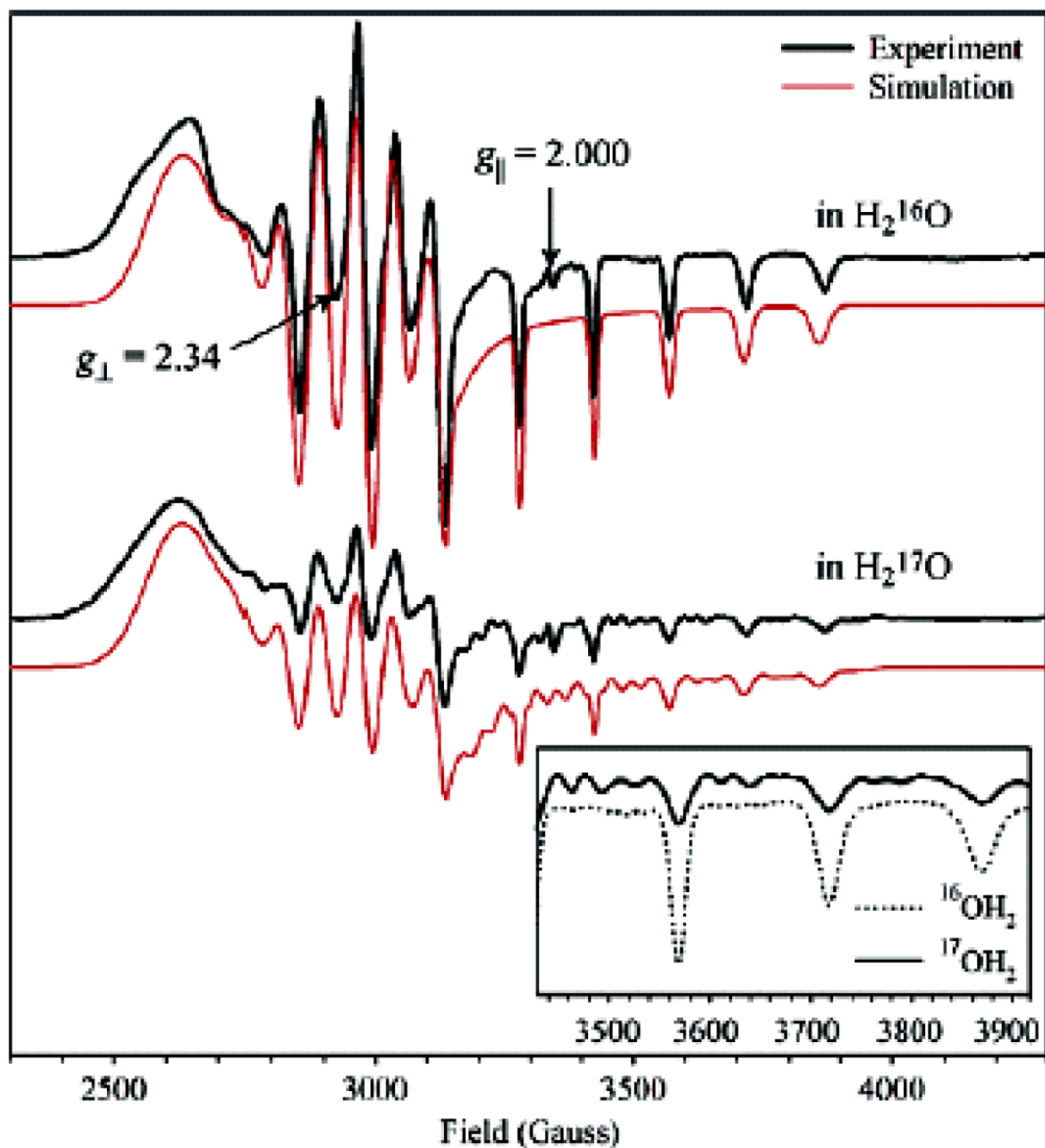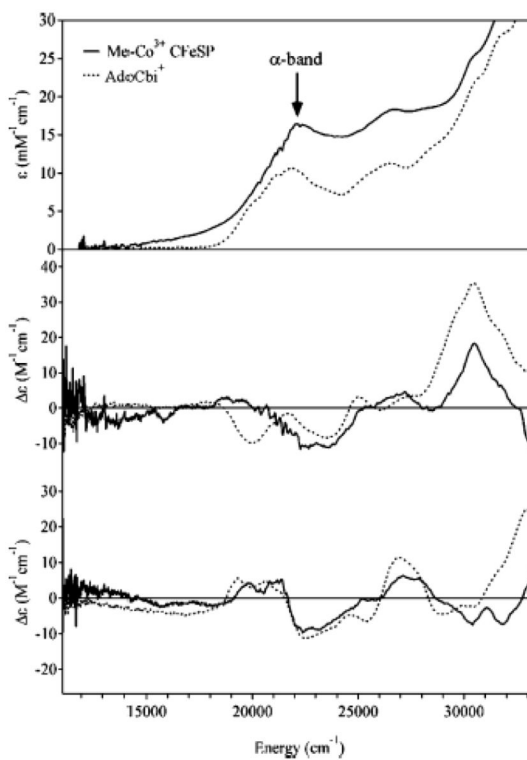
Figure 3.
Experimental (thick black lines) and simulated (thin red lines) X-band EPR spectra of $Co^{2+}CFeSP$ resuspended in natural abundance H_2O (top) and H_2 ^{17}O (bottom). Inset: Exploded view reveals additional features in the high-field region of the EPR spectrum of $Co^{2+}CFeSP$ resuspended in H_2 ^{17}O (solid line) compared to that resuspended in n.a. H_2O (dotted line). EPR spectra were recorded at 100 K using 9.39 GHz microwave frequency, 16 mW microwave power, 10.4 G modulation amplitude, and 100 kHz modulation frequency. Relevant EPR parameters and complete simulation input files are given in Table 2 and the Supporting Information, respectively.

Figure 4.
Comparison of 4.5 K Abs (top), 4.5 K CD (middle), and 7 T 100 K MCD (bottom) spectra of methylated CFeSP (solid lines) and AdoCbi$^+$ (dotted lines)
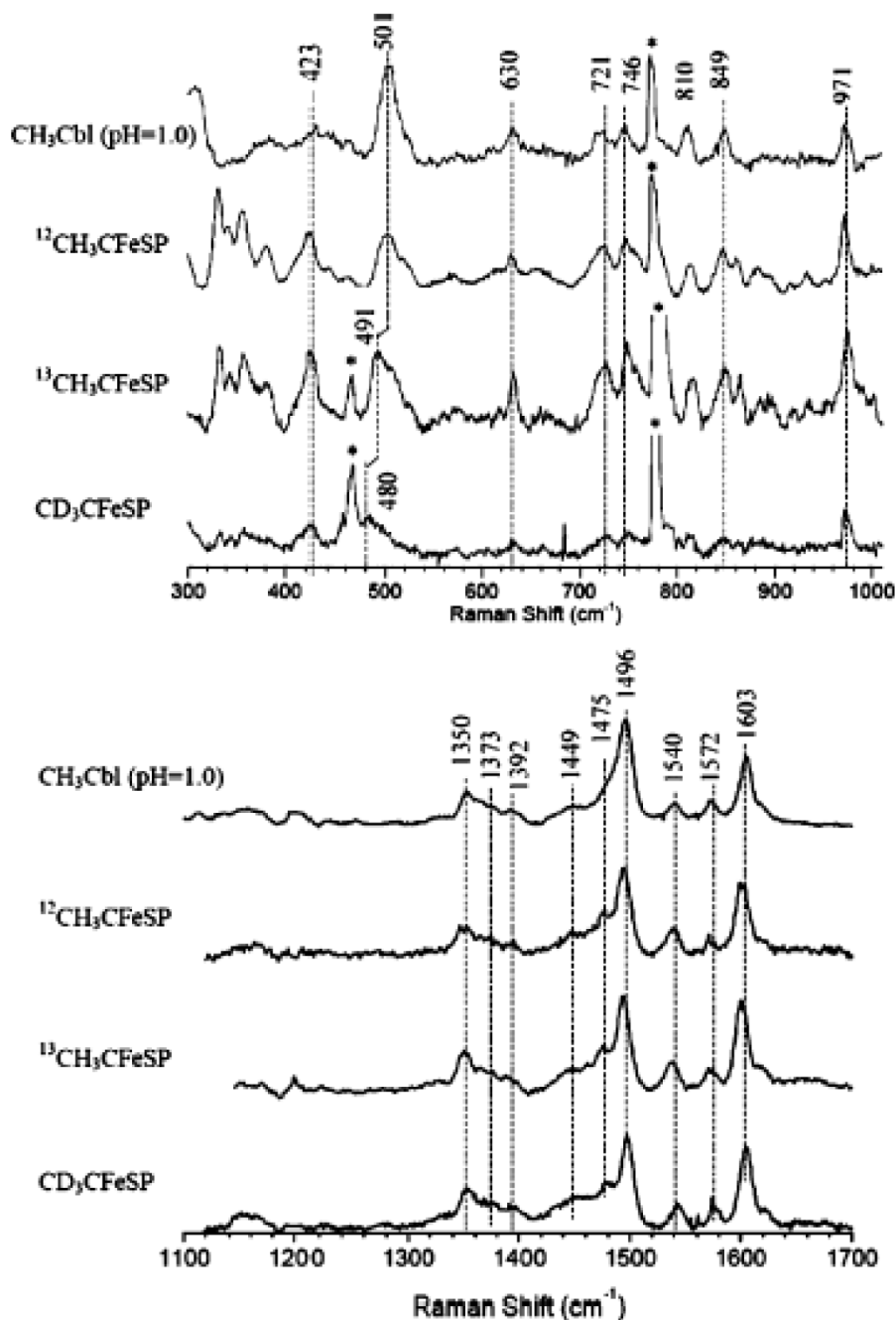
Figure 5.
Low-frequency (top panel) and high-frequency (bottom panel) regions of the resonance Raman spectra obtained for MeCbl at pH 1.0 (A), $^{12}CH_3$–CFeSP (B), $^{13}CH_3$–CFeSP (C), and CD$_3$–CFeSP (D). All data were collected at 77 K with 441.6 nm laser excitation
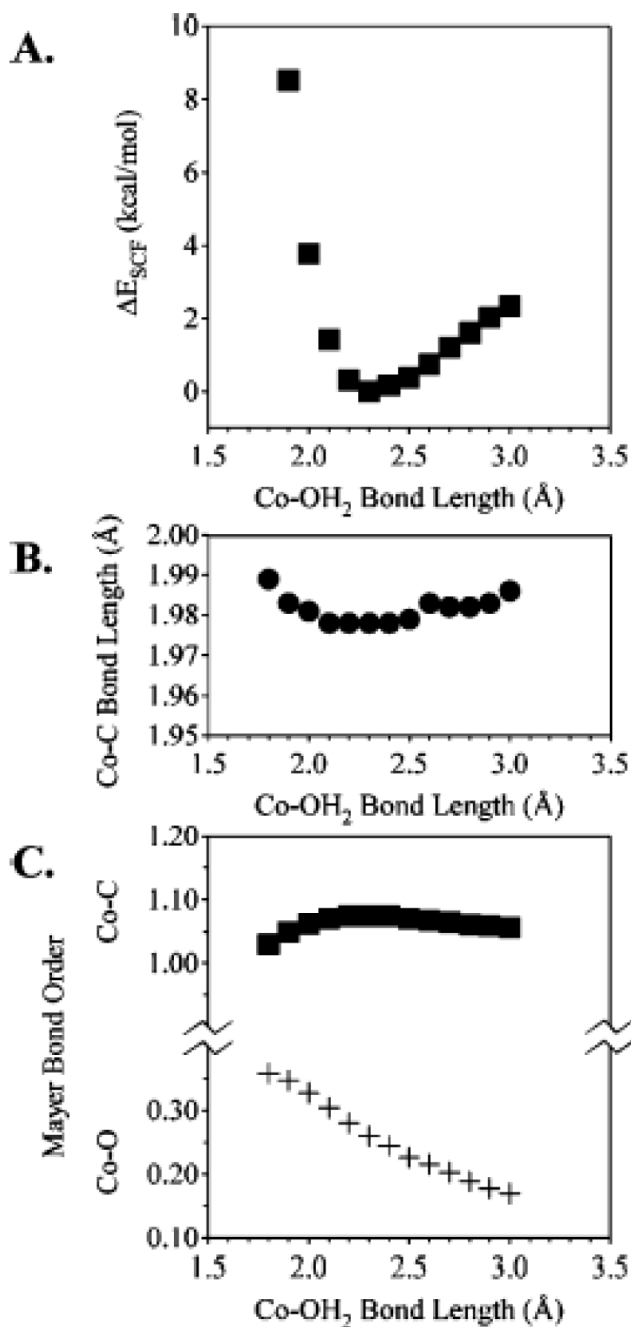
Figure 6.
Calculated potential energy surfaces (A), Co–CH$_3$ bond length (B), and nature of axial ligand bonding (C) as a function of Co–OH$_2$ bond length for a series of QM/MM optimized MeCbi$^+$ models.
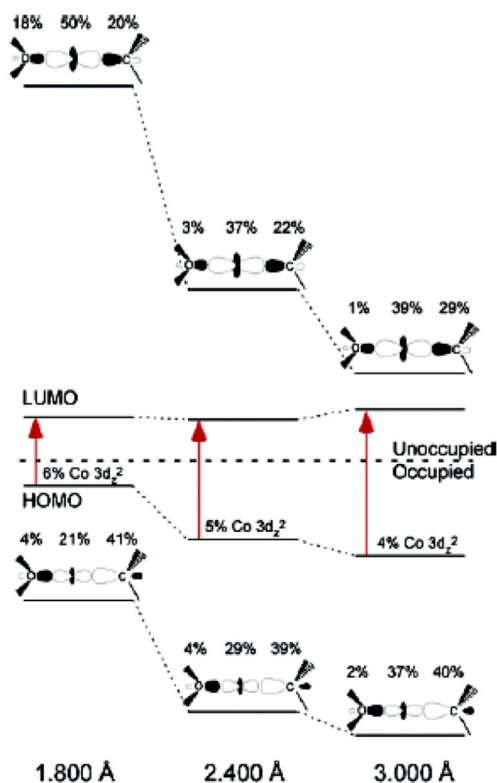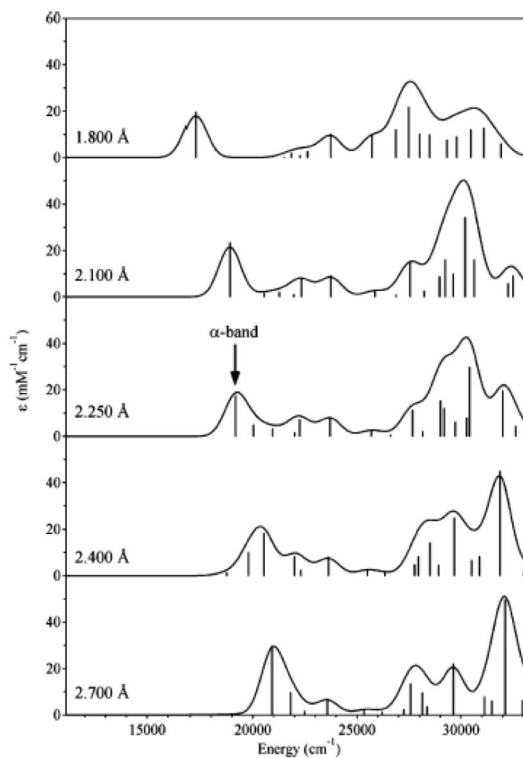
Figure 7.
Calculated MO diagram detailing the relative energies and compositions of the HOMO, LUMO, and orbitals involved in the dominant axial ligand bonding interactions for selected QM/MM optimized MeCbi$^+$ models with lower axial ligand Co–OH$_2$ bond lengths of 1.8 Å. (left), 2.4 Å (center), and 3.0 Å (right). The percent contributions from the Co 3d$_z$2, water 2p$_z$, and methyl 2p$_z$ orbitals are noted. Red arrows indicate the donor and acceptor MOs involved in the α-band transition predicted for each model using TD-DFT.

Figure 8.
TD-DFT/B3LYP predicted Abs spectra for QM/MM optimized MeCbi$^+$ models with lower axial ligand bond lengths fixed at values ranging from 1.800 to 2.700 Å. All calculated spectra were red-shifted by 3000 cm^{-1} to facilitate comparison with the experimental spectroscopic data presented above.

Table 1

Fit Parameters from a Gaussian Deconvolution of the Low-Energy Portion of the $Co^{2+}CFeSP$ MCD Spectrum [a]

band	energy (cm^{-1})	MCD Δε (M^{-1}cm^{-1})	ΔE (cm^{-1})
1	16,600	59.6	+150
2	17,700	99.7	+50
3	19,100	53.0	+200
4	19,850	53.9	0
5	21,000	160.4	0
6	21,600	−170.9	0
7	22,900	−114.4	0

[a]The ΔE values correspond to the shift in band positions from the $Co^{2+}Cbi^{+}$ to $Co^{2+}CFeSP$ MCD spectra.

Table 2

Co^{2+}CFeSP EPR Simulation Parameters

	g$_z$	g$_y$	g$_x$	A(^{59}Co), MHz			A(^{17}O), MHz		
				A$_z$	A$_y$	A$_x$	A$_z$	A$_y$	A$_x$
Co^{2+}Cbi^{+a}	1.999	2.338	2.338	405	220	220			
Co^{2+}CFeSP	2.000	2.340	2.340	406	230	230	−102	−89	−89

^{a}Reference 26.